



Article

High-Performance Biscrolled Ni-Fe Yarn Battery with Outer Buffer Layer

Jin Hyeong Choi ^{1,†}, Juwan Kim ^{1,†}, Jun Ho Noh ^{1,2}, Gyuyoung Lee ¹, Chaewon Yoon ¹, Ui Chan Kim ¹, In Hyeok Jang ¹, Hae Yong Kim ¹ and Changsoo Choi ^{1,3,*}

¹ Department of Energy and Materials Engineering, Dongguk University, 30 Pildong-ro, 1-gil, Jung-gu, Seoul 04620, Republic of Korea

² Department of Advanced Battery Convergence Engineering, Dongguk University, 30 Pildong-ro, 1-gil, Jung-gu, Seoul 04620, Republic of Korea

³ Research Center, Sillo Incorporation, 30 Pildong-ro, 1-gil, Jung-gu, Seoul 04620, Republic of Korea

* Correspondence: cschoi84@dongguk.edu

† These authors contributed equally to this work.

Abstract: The increasing demand for portable and wearable electronics has promoted the development of safe and flexible yarn-based batteries with outstanding electrochemical properties. However, achieving superior energy storage performance with a high active material (AM) load and long cycle life with this device format remains a challenge. In this study, a stable and rechargeable high-performance aqueous Ni-Fe yarn battery was constructed via biscrolling to embed AMs within helical carbon nanotube (CNT) yarn corridors. Owing to the high load of charge storage nanoparticles (NPs; above 97 wt%) and the outer neat CNT layer, the buffered biscrolled Ni-Fe yarn battery demonstrates excellent linear capacity (0.053 mAh/cm) and cycling stability (60.1% retention after 300 charge/discharge cycles) in an aqueous electrolyte. Moreover, our flexible yarn battery exhibits maximum energy/power densities of 422 mWh/cm³ and 7535 mW/cm³ based on the total volume of the cathode and anode, respectively, which exceed those reported for many flexible Ni-Fe batteries. Thus, biscrolled Ni-Fe yarn batteries are promising candidates for next-generation conformal energy solutions.

Keywords: biscrolled yarn; Ni-Fe batteries; high load; durability; carbon nanotubes



Citation: Choi, J.H.; Kim, J.; Noh, J.H.; Lee, G.; Yoon, C.; Kim, U.C.; Jang, I.H.; Kim, H.Y.; Choi, C. High-Performance Biscrolled Ni-Fe Yarn Battery with Outer Buffer Layer. *Int. J. Mol. Sci.* **2023**, *24*, 1067. <https://doi.org/10.3390/ijms24021067>

Academic Editor: Andreas Taubert

Received: 16 December 2022

Revised: 29 December 2022

Accepted: 3 January 2023

Published: 5 January 2023



Copyright: © 2023 by the authors. Licensee MDPI, Basel, Switzerland. This article is an open access article distributed under the terms and conditions of the Creative Commons Attribution (CC BY) license (<https://creativecommons.org/licenses/by/4.0/>).

1. Introduction

Owing to the increasing demand for personal health-monitoring devices, intelligent garments, rollup displays, and implantable medical devices, researchers have made considerable progress in the field of flexible and wearable electronics over the past few years [1–6]. Because of a rapidly growing market, researchers are increasingly interested in different kinds of fibrous power sources such as lithium-ion batteries, zinc-ion batteries, primary batteries, and supercapacitors for the development of 1D linear energy storage devices [7–16]. For example, lightweight, flexible, and wearable yarn-based aqueous batteries with tiny volumes are one of the most fascinating candidates for wearable electronics [17–22].

Researchers and engineers have tried many strategies to manufacture yarn-shaped batteries: for example, chemical vapor deposition, hydrothermal synthesis, electrodeposition, and in situ polymerization [23–28]. Nevertheless, producing high-performance fibrous batteries with a sufficient mass load and long cycle life remains a challenge [29–31]. The biscrolling method, which enables the straightforward incorporation of active materials (AMs) into carbon nanotubes (CNTs), is an eminent choice, as it maximizes the AM load (>90 wt%) without the need for binders and laborious procedures [32,33]. Thus, various AMs can be integrated into flexible CNT-based yarn-structured batteries. The easy control of the diameter and porosity of the yarn

provides the AMs with steady access to the electrolyte. More importantly, wearable batteries must be suitable for the direct contact with human skin; they should not explode or ignite. Aqueous Ni–Fe batteries, which are traditional aqueous batteries, are relatively safe and cost-effective and exhibit high energy densities [34,35].

In this study, we built a flexible biscrolled Ni–Fe yarn battery (i.e., “BNF yarn battery”) with a Ni(OH)₂ cathode, Fe₃O₄ anode, and water-based electrolyte. Owing to the high AM content (Ni content: up to 98.5 wt%; Fe content: up to 97.4 wt%), the fabricated BNF yarn battery with 1.1 V voltage provides a linear capacity of 0.053 mAh/cm at 0.1 mA/cm current density in an aqueous electrolyte. Because of the outer neat CNT buffer layer, our BNF yarn battery exhibits 60.1% capacity retention for over 300 cycles with high coulombic efficiency. This results in a high energy density of 422 mWh/cm³ and a high power density of 7535 mW/cm³, which are better than those of the most previously reported flexible Ni–Fe batteries. The proof-of-concept incorporation of mechanically flexible BNF yarn batteries with these properties into textiles renders them promising candidates for wearable electronics.

2. Results

2.1. Preparation and Morphology of Biscrolled AM/CNT Yarns

We employed CNT sheets that were drawn from spinnable CNT forests [36] as the host material to form a twist-spun yarn. The guest-free neat CNT yarns (Figure 1(i)) have highly oriented and porous structures (Figure S1); thus, active guest materials can be trapped within the CNT network. We fabricated the biscrolled AM/CNT yarns (Figure 1(ii)) with the typical biscrolling method [33]: an AM/CNT hybrid sheet stack was prepared by drop-casting a dispersion of charge storage nanoparticles (NPs) onto stacked CNT sheets and spinning them at approximately 1200 turns/m. The resulting NP load was tuned by varying the AM concentration that was dispersed in the ethanol. More importantly, the outermost layer of the as-fabricated biscrolled yarn was wrapped into neat CNT sheets to ensure the anchoring of the AMs (Figure S2); that is, the CNT wrapping layer serves as a buffer layer that prevents the AMs from being desorbed during the electrochemical reaction. Thereby, the buffered biscrolled AM/CNT yarns (i.e., the b-biscrolled AM/CNT yarns) are expected to exhibit a high energy storage capacity and excellent cycling durability owing to the maximized weight percentage of the guest without compromising the accessibility of the electrolyte to the guest.

More specifically, 98.5 wt% Ni(OH)₂ NPs and 97.4 wt% Fe₃O₄ NPs were embedded as the AMs in the cathode and anode yarns, respectively. The scanning electron microscopy (SEM) images of the surface and magnified area of the guest NP-loaded biscrolled yarn are shown in Figure 1b,c. Despite the low content of the CNT host, the guest materials are embedded within the CNT scroll galleries. Moreover, a considerable amount of partially aggregated guest material resides on the biscrolled yarn surface, leaving the possibility of a detachment of the AMs. These biscrolled yarns exhibit stable electrical resistance (approximately 90 ohm/cm) irrespective of the AM type, which represents the resistance of the CNT host (Figure 1d). Moreover, a 5 cm long and 200 μm thick biscrolled Ni/CNT yarn was attached to a conductive film and used in an electrical circuit (Figure 1e). The biscrolled yarn provided the blue light-emitting diode (LED) in the circuit with power even when a glass vial filled with water was attached to the yarn (30 g, which is ten thousand times heavier than the yarn); thus, the yarn possesses superior mechanical properties even at a high load of brittle guest NPs. In addition, the as-prepared biscrolled yarn was strong and flexible enough to be (i) straightened, (ii) plied, and (iii) wound around a 2 mm diameter glass tube, as shown in Figure 1f.

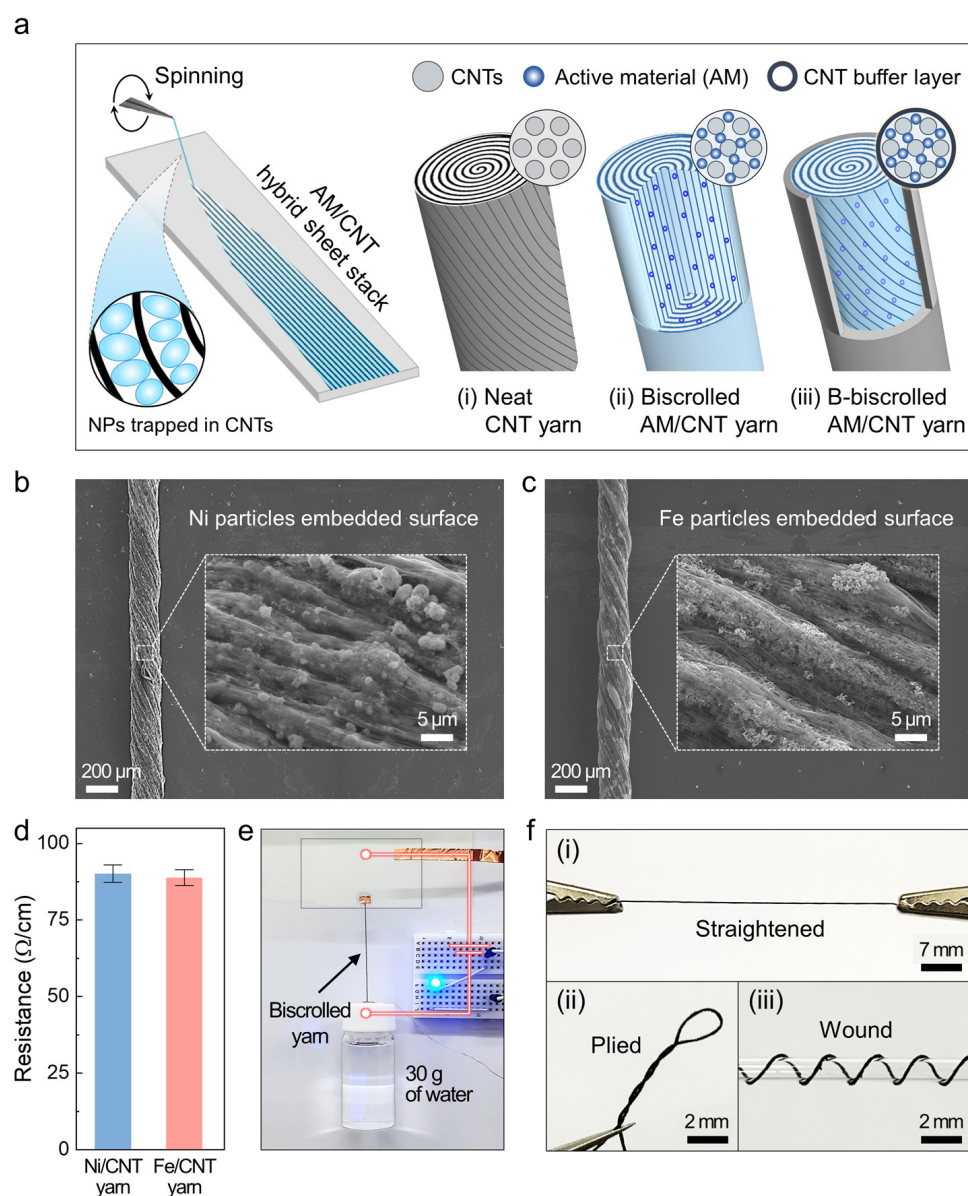


Figure 1. Fabrication of a biscallored AM/CNT yarn with outer buffer layer. (a) Schematic of fabrication of biscallored AM/CNT yarns. The AM/CNT hybrid sheets were scrolled and wrapped into a neat CNT layer to build a buffered biscallored AM/CNT yarn (i.e., a b-biscallored AM/CNT yarn) in which the AM NPs are uniformly distributed within the CNT framework. The SEM images and magnified areas (insets) show the surfaces of (b) a 98.5 wt% Ni-embedded cathode yarn and (c) a 97.4 wt% Fe-embedded anode yarn. (d) Length-normalized resistances of biscallored Ni/CNT (blue bar) and Fe/CNT (red bar) yarns. (e) A biscallored Ni/CNT yarn bearing a 30 g glass vial filled with water is connected to a power source to power a blue LED. (f) Photographs of (i) straightened and (ii) plied biscallored Ni/CNT yarns and (iii) those wound around a glass tube.

2.2. Electrochemical Properties of the BNF Yarn Battery

The electrochemical properties of the $\text{Ni}(\text{OH})_2$ cathode and Fe_3O_4 anode were determined with cyclic voltammetry (CV) experiments in the three-electrode configuration with a 6M potassium hydrate (KOH) solution. Figure S3a shows a pair of redox peaks of $\text{Ni}(\text{OH})_2$ at 0–0.55 V versus Ag/AgCl reference electrode, which correspond to the reversible redox reactions between Ni^{2+} and Ni^{3+} with OH^- [37,38]. As shown in Figure S3b, the CV curves of Fe_3O_4 display one dominant pair of redox peaks (at approximately –1.1 and –0.7 V) and other small peaks (at approximately –0.8 V), which originate from the redox reaction

between $\text{Fe}^{2+}/\text{Fe}^{3+}$ and Fe^0 with OH^- . This result agrees well with previously published results for Fe_3O_4 -based electrodes [39]. Based on these results, BNF yarn-based full cells were fabricated with the $\text{Ni}(\text{OH})_2/\text{CNT}$ biscrolled yarn as the cathode and the $\text{Fe}_3\text{O}_4/\text{CNT}$ biscrolled yarn as the anode in aqueous electrolyte (Figure S4). The linear capacity versus the mass ratio of Ni/Fe is presented in Figure S5. The optimal $\text{Ni}(\text{OH})_2/\text{Fe}_3\text{O}_4$ mass ratio is 1.8 for a reasonable and excellent charge balance between the cathode and anode. Figure S6 shows typical CV curves of the BNF yarn battery for different scan rates. The well-defined pair of redox peaks indicates good agreement with the following reaction in the Ni-Fe battery system [40]:



The CV curve of the b-BNF yarn battery exhibits a similar trend at the presented scan rates, thereby indicating that the electrolyte sufficiently penetrated the biscrolled yarn and that the embedded AMs could fully participate in the electrochemical reactions with sufficient contact to the electrolyte. Thereby, the BNF and b-BNF yarn batteries provided similar specific capacities (from 22.5 to 59.3 mAh/g based on the total mass of the AMs) and rate capacities at different scan rates (Figure 2b). The specific capacity (C_{sp}) was calculated from the CV curves using the following equation: $C_{\text{sp}}(\text{mAh/g}) = \int i/\text{mdt}$, where i is the oxidation or reduction current, dt is the time differential, and m is the total mass of the AMs. In addition, both had similar discharge plateaus and periods (Figure 2c). These results confirm that the neat CNT sheath has no noticeable influence on the capacity of the BNF yarn battery. Evidently, the CNT layer only functions as a buffer layer without participating in the electrochemical reaction of the Ni-Fe battery. The effect of the CNT buffer layer on the electrochemical performance was further investigated with electrochemical impedance spectroscopy (EIS; Figure 2d). Its Nyquist plots (frequency range from 10 Hz to 100 kHz) clearly show that both the equivalent series resistance (i.e., the intersection of the curve at the real part) and the inclined curve in the low-frequency region (i.e., the ion diffusion impedance) of the BNF yarn battery substantially overlapped with those of the b-BNF yarn battery. Furthermore, both batteries revealed the absence of a semicircle in the high-frequency range, thereby indicating the high conductivity of the yarns and the low charge transfer resistance. Notably, the low impedance at 10 Hz ($<200 \Omega$) implies that the ions could easily enter the biscrolled yarn from the aqueous electrolyte even with a CNT buffer layer. More specifically, the series resistance of the b-biscrolled yarn at 100 kHz was 13.3Ω and, thereby, lower than that of the biscrolled yarn (13.6Ω ; inset of Figure 2d). This slight reduction due to the additional CNT wrapping layer can be explained by the fact that the CNTs provide an enhanced conductive network and promote electron transport.

The electrochemical stability of Ni-Fe batteries is a great concern regarding their widespread commercialization. The cycling performance of our b-BNF yarn batteries was investigated by repeatably charging/discharging them at 0.1 mA/cm . As shown in Figure 2e, the b-BNF yarn battery retained approximately 60.1% of its initial capacity after 300 cycles, whereas the BNF yarn battery showed a short cycle life with only approximately 20.2% capacity retention. The slight increase in the capacity in the initial stage can be attributed to the progressive permeation of the electrolyte with the activation of the AMs [37,41]. The improved durability comes from the protecting neat CNT sheath; the effect is similar to the previously reported buffering behavior of PEDOT shells [42]. Figure 2f shows the linear capacity and capacity retention versus the number of outer CNT buffer layers. It should be noted that the linear capacity of approximately 0.053 mAh/cm remained almost unchanged despite the increase in the number of buffer layers, while the capacity retention rate gradually increased. The buffering effect of the outermost CNT layers was confirmed by taking optical images of the yarns before and after the cycling test. According to Figure 2g, a large amount of exposed Ni particles on the surface of the biscrolled yarn was completely covered by the CNT buffer layer, which resulted in good dissolution tolerance to the electrolyte solution. The biscrolled Ni/CNT yarn without the

outer buffer experienced evident Ni particle desorption after 300 cycles, and its surface became smooth (Figure S7, upper image). By contrast, the surface morphology of the b-biscrolled Ni/CNT yarn was well preserved (Figure S7, lower image). Figure 2h presents the predicted dissolution model of the AM NPs embedded in the biscrolled yarns. In the case of the biscrolled yarn without the external buffer, the AM may be desorbed through the yarn surface into the electrolyte because of the aggressive electrochemical reaction. This adverse effect does not occur in the biscrolled yarn with the outer buffer layer, which confines the AM in the yarn.

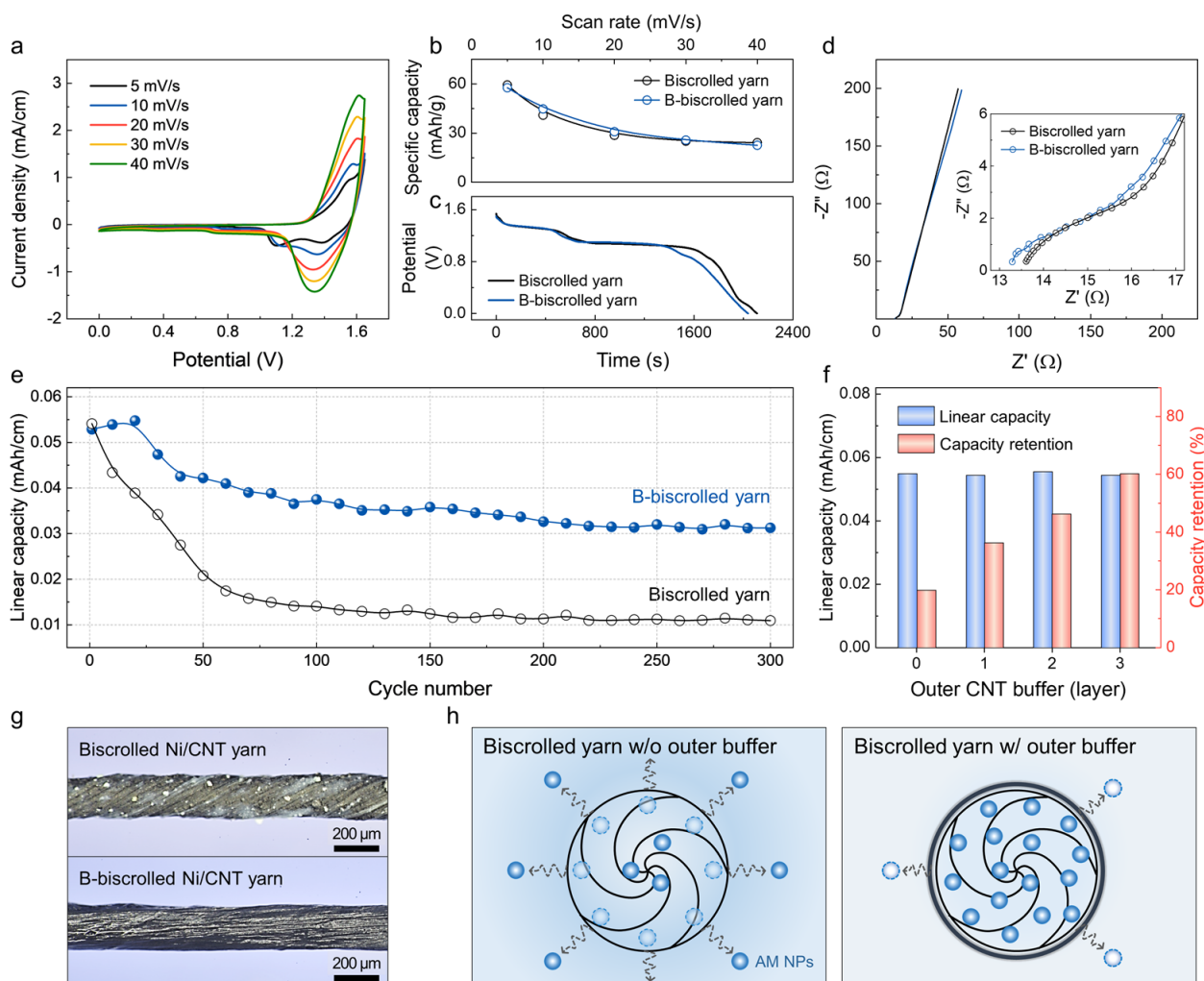


Figure 2. Electrochemical characterizations of the BNF yarn batteries. (a) CV curves of b—BNF yarn battery in aqueous 6M KOH at different scan rates. (b) Average specific capacity as a function of the scan rate, (c) galvanostatic discharge curves at 0.1 mA/cm, (d) Nyquist plots (from 10 Hz to 100 kHz), and (e) cycling stability of BNF and b—BNF yarn batteries at 0.1 mA/cm. Inset in d shows enlarged section of Nyquist plots. (f) Dependence of linear capacity and capacity retention on outer CNT buffer layer. (g) Optical images show biscrolled Ni/CNT yarn (top) and b—biscrolled Ni/CNT yarn (bottom). (h) Schematics show the expected AM NP desorption process (indicated by arrows) of the biscrolled yarns without (left) and with (right) an outer CNT buffer layer in an aqueous electrolyte.

2.3. Performance and Practical Applications

In this work, the amount of AMs in the yarn was controlled by altering their dispersion concentrations; this resulted in a volumetric loading density and corresponding linear capacity of 2.26 g/cm³ and 0.053 mAh/cm, respectively (Figure 3a). This high load can be ascribed to the strong compressive forces generated by the inserted twists [33]. The galvanostatic

static discharge curves measured at different current densities (from 0.1 to 1 mA/cm) and the corresponding capacity retention rate against the number of charge/discharge cycles are presented in Figures 3b and 3c, respectively. All curves display distinct discharge voltage plateaus at approximately 1.1 V, which are consistent with the CV curves in Figure 2a. This b-BNF yarn battery exhibited a high linear capacity of 0.053 mAh/cm at 0.1 mA/cm current density and 0.031 mAh/cm at 1 mA/cm current density, thereby indicating its good rate capability. In addition, the coulombic efficiency was approximately 100% during rate cycling; hence, the battery is a feasible power supply [40,43,44]. More importantly, when the total volume of the cathode and anode is considered, our b-BNF yarn battery yielded an incredibly high energy density of 422 mWh/cm³ at 753 mW/cm³ power density. Even at 7535 mW/cm³, the energy density was 229 mWh/cm³. Thus, the proposed b-BNF yarn battery outperforms most previously reported Ni-Fe batteries (Figure 3d) [45–53].

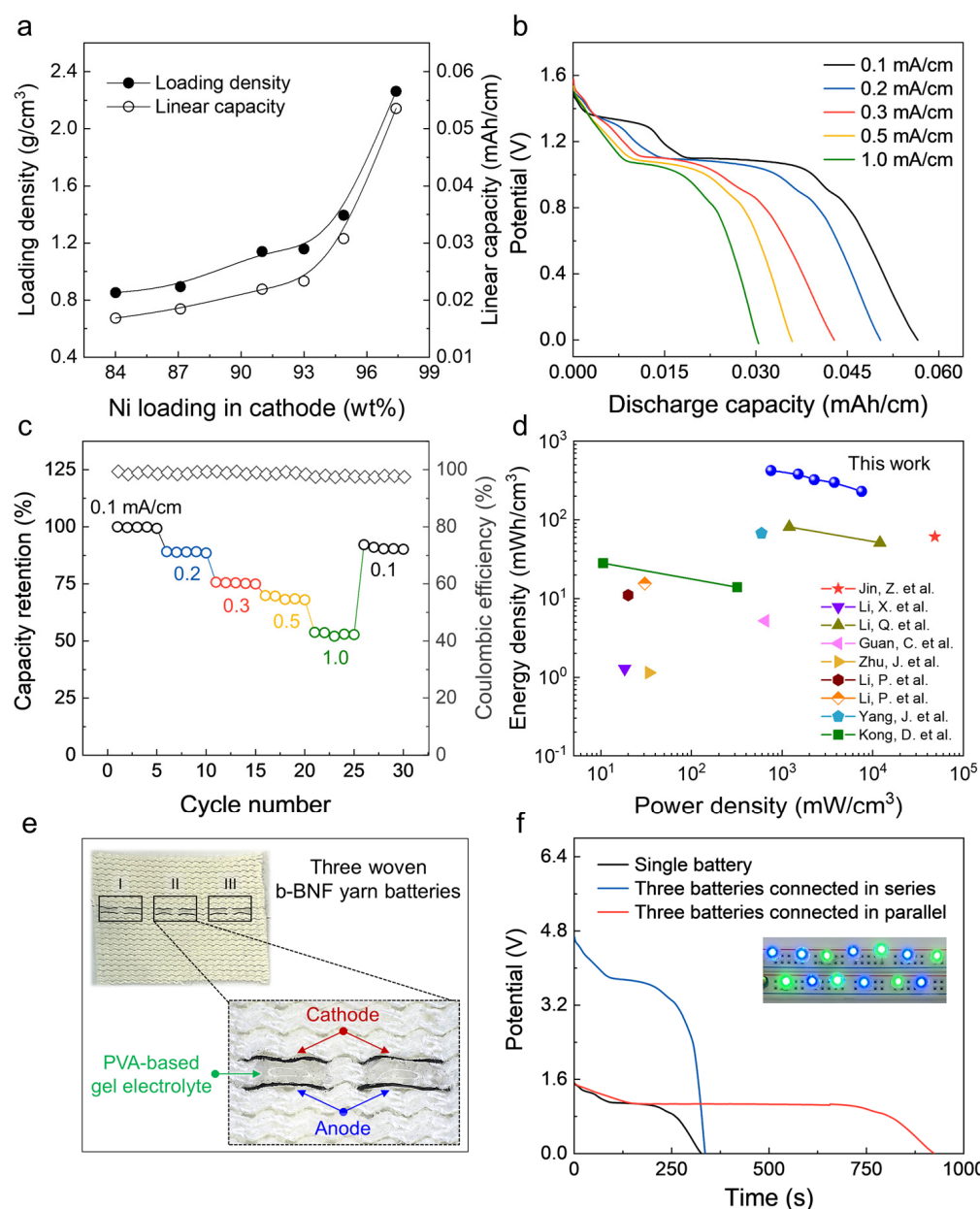


Figure 3. Performances of the b-BNF yarn batteries and demonstration as a practical power source. (a) Linear capacity versus Fe load in anode (Ni-to-Fe mass ratio is 1.8:1). (b) Galvanostatic discharge

curves at different current densities. (c) Capacity retention and corresponding coulombic efficiency of b-BNF yarn battery. (d) Ragone plot of as-fabricated Ni-Fe battery (based on total volume of the cathode and anode) [45–53]. (e) Photographs showing three b-BNF yarn batteries woven into a commercial textile. Inset shows that each cell consists of a 3 cm-long Ni(OH)₂ cathode yarn and a 3 cm-long Fe₃O₄ anode yarn with a gel electrolyte (PVA-KOH). (f) Galvanostatic discharge curves of single b-BNF yarn battery (black curve) and three batteries connected in series (blue curve) and parallel (red curve) at 1 mA/cm. The inset shows 13 LEDs (seven blue and six green) illuminated by three serial-connected b-BNF yarn batteries.

To demonstrate the viability for power source application in wearable electronic devices, the three b-BNF yarn batteries were assembled in series or parallel. Figure 3e exhibits that 3 cm long, three b-BNF yarn batteries can be woven into a commercial textile with a poly(vinyl alcohol) (PVA) gel electrolyte owing to their mechanical strength and flexibility. According to the discharge curves (Figure 3f), the voltage and capacity are tripled for the serial (blue line) and parallel (red line) assemblies, respectively, thereby increasing the power and energy output. Because of their high energy/power density, the woven BNF yarn batteries can simultaneously power and light up seven blue LEDs and six green LEDs with a dazzling brightness (inset of Figure 3f).

3. Materials and Methods

3.1. Chemicals

For the yarn electrode materials, aerogel multiwalled CNT sheets were drawn from 320 μm high CNT forests (A-Tech System Co., Hwaseong-si, Korea). Regarding the AMs for energy storage, the cathode and anode contained commercially available Ni(OH)₂ powder with 1 μm particle diameter and Fe₃O₄ powder with 50–100 nm particle diameter, respectively.

In addition, 6M KOH aqueous electrolyte was prepared by dissolving 33.6 g KOH in 100 mL deionized water. To prepare the PVA+KOH solid gel electrolyte, 2 g PVA and 6.7 g KOH were mixed in 20 mL deionized water. The PVA + KOH solution was stirred at 130 °C until it was transparent and viscous.

3.2. Preparation Biscrolled Yarn Battery and B-Biscrolled Yarn Battery

Four 10 mm wide and 75 mm long CNT sheets were stacked onto a glass plate. To add the AMs onto the CNT sheets, their powders were dispersed in ethanol and dropped onto the CNT sheets; subsequently, the samples were dried at room temperature. To convert 2D sheets into flexible 1D yarn, one end of the AM/CNT sheets was attached to the electrical motor and twisted at approximately 1200 turns/m. Afterward, the parallel biscrolled yarn cathode and anode were connected to copper wires with silver paste and coated with epoxy to prevent unwanted electrochemical side reactions. The b-biscrolled yarn was prepared by wrapping the yarn into the CNT buffer layer; it consisted of three layers of 10 mm wide and 75 mm long CNT sheets that had parallelly been drawn on a vernier caliper (Mitutoyo, Japan). The prepared biscrolled yarn was placed on it. In the next step, the sample was rolled into a cylindrical cone. This cone was densified by inserting twists (approximately 500 turns) and dropping ethanol onto the yarn.

3.3. Characterization

The morphological information was obtained with SEM (S-4600, Hitachi, Japan) and optical microscopy (D750, Nikon, Japan). In addition, an electrochemical analyzer (Vertex EIS, Ivium) was used for all the electrochemical measurements.

3.4. Electrochemical Calculation

The weight of the AM wt% was calculated as follows:

$$wt\% = \frac{W_{total} - W_{CNT}}{W_{total}} \times 100 = \frac{W_{AM}}{W_{total}} \times 100$$

where wt% is the weight percentage of the AM NPs, W_{total} is the total weight of the biscrolled yarn battery, W_{CNT} is the weight of neat CNT yarn, and W_{AM} is the weight of the AM NPs. The loading density was calculated by normalizing W_{AM} to the volume of the biscrolled yarn.

The capacity was calculated as follows:

$$Capacity = \frac{I_{discharge} \cdot \Delta t}{Unit}$$

where $I_{discharge}$ is the discharge current, Δt is the discharge time, and $Unit$ is the length, volume, area, and mass of the yarn battery.

4. Conclusions

We built high-performance aqueous Ni-Fe yarn batteries by embedding AMs into the inner structure of helical CNT yarns. The employed biscrolling technique enabled the high loading of AMs onto the cathode (Ni: up to 98.5 wt%) and anode (Fe: up to 97.4 wt%). These highly loaded BNF yarn-based batteries delivered a maximum energy density of 422 mWh/cm³ and a power density of 7535 mW/cm³; thereby, they perform better than most previously reported Ni-Fe batteries. More importantly, owing to the introduction of external CNT buffer layers, the b-BNF yarn battery can retain up to 60.1% of its initial large linear capacity (0.053 mAh/cm) even after 300 charge/discharge cycles with almost 100% coulombic efficiency. Therefore, the presented high-performance b-BNF yarn battery is a promising next-generation energy source for wearable and portable electronics.

Supplementary Materials: The following supporting information can be downloaded at: <https://www.mdpi.com/article/10.3390/ijms24021067/s1>.

Author Contributions: J.H.C., J.K. and C.C. conceived the idea and performed the experiments. J.H.N., G.L., C.Y. and U.C.K. analyzed the experimental results. I.H.J. and H.Y.K. designed the experiment. J.H.C. and J.K. contributed equally to this work. All authors have read and agreed to the published version of the manuscript.

Funding: This research received no external funding.

Institutional Review Board Statement: Not applicable.

Informed Consent Statement: Not applicable.

Data Availability Statement: Not applicable.

Acknowledgments: This work was supported by the Basic Science Research Programs through the National Research Foundation of Korea (NRF-2022R1F1A1064550). This work was also supported by the Korea Institute of Energy Technology Evaluation and Planning (KETEP) and the Ministry of Trade, Industry & Energy (MOTIE) of the Republic of Korea (No. 2022400000020).

Conflicts of Interest: The authors declare no conflict of interest.

References

1. Wen, Z.; Yeh, M.-H.; Guo, H.; Wang, J.; Zi, Y.; Xu, W.; Deng, J.; Zhu, L.; Wang, X.; Hu, C.; et al. Self-powered textile for wearable electronics by hybridizing fiber-shaped nanogenerators, solar cells, and supercapacitors. *Sci. Adv.* **2016**, *2*, e1600097. [[CrossRef](#)] [[PubMed](#)]
2. Zamarayeva, A.M.; Ostfeld, A.E.; Wang, M.; Duey, J.K.; Deckman, I.; Lechêne, B.P.; Davies, G.; Steingart, D.A.; Arias, A.C. Flexible and stretchable power sources for wearable electronics. *Sci. Adv.* **2017**, *3*, e1602051. [[CrossRef](#)] [[PubMed](#)]
3. Chen, J.; Liang, J.; Zhou, Y.; Sha, Z.; Lim, S.; Huang, F.; Han, Z.; Brown, S.A.; Cao, L.; Wang, D.W.; et al. A vertical graphene enhanced Zn-MnO₂ flexible battery towards wearable electronic devices. *J. Mater. Chem. A* **2021**, *9*, 575–584. [[CrossRef](#)]
4. Xiang, X.; Zhang, K.; Chen, J. Recent Advances and Prospects of Cathode Materials for Sodium-Ion Batteries. *Adv. Mater.* **2015**, *27*, 5343–5364. [[CrossRef](#)] [[PubMed](#)]
5. Liu, Q.-C.; Xu, J.-J.; Xu, D.; Zhang, X.-B. Flexible lithium-oxygen battery based on a recoverable cathode. *Nat. Commun.* **2015**, *6*, 7892. [[CrossRef](#)] [[PubMed](#)]

6. Yu, D.; Goh, K.; Wang, H.; Wei, L.; Jiang, W.; Zhang, Q.; Dai, L.; Chen, Y. Scalable synthesis of hierarchically structured carbon nanotube–graphene fibres for capacitive energy storage. *Nat. Nanotechnol.* **2014**, *9*, 555–562. [[CrossRef](#)]
7. Kwon, Y.H.; Woo, S.-W.; Jung, H.-R.; Yu, H.K.; Kim, K.; Oh, B.H.; Ahn, S.; Lee, S.-Y.; Song, S.-W.; Cho, J.; et al. Cable-Type Flexible Lithium Ion Battery Based on Hollow Multi-Helix Electrodes. *Adv. Mater.* **2012**, *24*, 5192–5197. [[CrossRef](#)]
8. Hoshida, T.; Zheng, Y.; Hou, J.; Wang, Z.; Li, Q.; Zhao, Z.; Ma, R.; Sasaki, T.; Geng, F. Flexible Lithium–Ion Fiber Battery by the Regular Stacking of Two-Dimensional Titanium Oxide Nanosheets Hybridized with Reduced Graphene Oxide. *Nano Lett.* **2017**, *17*, 3543–3549. [[CrossRef](#)]
9. Wang, Y.; Chen, C.; Xie, H.; Gao, T.; Yao, Y.; Pastel, G.; Han, X.; Li, Y.; Zhao, J.; Fu, K.; et al. 3D-Printed All-Fiber Li-Ion Battery toward Wearable Energy Storage. *Adv. Funct. Mater.* **2017**, *27*, 1703140. [[CrossRef](#)]
10. Huang, Y.; Ip, W.S.; Lau, Y.Y.; Sun, J.; Zeng, J.; Yeung, N.S.S.; Ng, W.S.; Li, H.; Pei, Z.; Xue, Q.; et al. Weavable, Conductive Yarn-Based NiCo//Zn Textile Battery with High Energy Density and Rate Capability. *ACS Nano* **2017**, *11*, 8953–8961. [[CrossRef](#)]
11. Wang, K.; Zhang, X.; Han, J.; Zhang, X.; Sun, X.; Li, C.; Liu, W.; Li, Q.; Ma, Y. High-Performance Cable-Type Flexible Rechargeable Zn Battery Based on MnO₂@CNT Fiber Microelectrode. *ACS Appl. Mater. Interfaces* **2018**, *10*, 24573–24582. [[CrossRef](#)] [[PubMed](#)]
12. Wang, Z.; Ruan, Z.; Liu, Z.; Wang, Y.; Tang, Z.; Li, H.; Zhu, M.; Hung, T.F.; Liu, J.; Shi, Z.; et al. A flexible rechargeable zinc-ion wire-shaped battery with shape memory function. *J. Mater. Chem. A* **2018**, *6*, 8549–8557. [[CrossRef](#)]
13. Li, M.; Meng, J.; Li, Q.; Huang, M.; Liu, X.; Owusu, K.A.; Liu, Z.; Mai, L. Finely Crafted 3D Electrodes for Dendrite-Free and High-Performance Flexible Fiber-Shaped Zn–Co Batteries. *Adv. Funct. Mater.* **2018**, *28*, 1802016. [[CrossRef](#)]
14. Zhang, Q.; Wang, X.; Pan, Z.; Sun, J.; Zhao, J.; Zhang, J.; Zhang, C.; Tang, L.; Luo, J.; Song, B.; et al. Wrapping Aligned Carbon Nanotube Composite Sheets around Vanadium Nitride Nanowire Arrays for Asymmetric Coaxial Fiber-Shaped Supercapacitors with Ultrahigh Energy Density. *Nano Lett.* **2017**, *17*, 2719–2726. [[CrossRef](#)] [[PubMed](#)]
15. He, N.; Shan, W.; Wang, J.; Pan, Q.; Qu, J.; Wang, G.; Gao, W. Mordant inspired wet-spinning of graphene fibers for high performance flexible supercapacitors. *J. Mater. Chem. A* **2019**, *7*, 6869–6876. [[CrossRef](#)]
16. Khudiyev, T.; Lee, J.T.; Cox, J.R.; Argentieri, E.; Loke, G.; Yuan, R.; Noel, G.H.; Tataru, R.; Yu, Y.; Logan, F.; et al. 100 m Long Thermally Drawn Supercapacitor Fibers with Applications to 3D Printing and Textiles. *Adv. Mater.* **2020**, *32*, e2004971. [[CrossRef](#)]
17. Mo, F.; Liang, G.; Huang, Z.; Li, H.; Wang, D.; Zhi, C. An overview of fiber-shaped batteries with a focus on multifunctionality, scalability, and technical difficulties. *Adv. Mater.* **2020**, *32*, 1902151. [[CrossRef](#)]
18. Li, Y.; Fu, J.; Zhong, C.; Wu, T.; Chen, Z.; Hu, W.; Amine, K.; Lu, J. Recent Advances in Flexible Zinc-Based Rechargeable Batteries. *Adv. Energy Mater.* **2018**, *9*, 1802605. [[CrossRef](#)]
19. Tebyetekerwa, M.; Marriam, I.; Xu, Z.; Yang, S.; Zhang, H.; Zabihi, F.; Jose, R.; Peng, S.; Zhu, M.; Ramakrishna, S. Critical insight: Challenges and requirements of fibre electrodes for wearable electrochemical energy storage. *Energy Environ. Sci.* **2019**, *12*, 2148–2160. [[CrossRef](#)]
20. Zhang, Y.; Zhao, Y.; Ren, J.; Weng, W.; Peng, H. Advances in Wearable Fiber-Shaped Lithium–Ion Batteries. *Adv. Mater.* **2016**, *28*, 4524–4531. [[CrossRef](#)]
21. Wang, M.; Xie, S.; Tang, C.; Zhao, Y.; Liao, M.; Ye, L.; Wang, B.; Peng, H. Making fiber-shaped Ni//Bi battery simultaneously with high energy density, power density, and safety. *Adv. Funct. Mater.* **2020**, *30*, 1905971. [[CrossRef](#)]
22. Zhang, Y.; Jiao, Y.; Lu, L.; Wang, L.; Chen, T.; Peng, H. An Ultraflexible Silicon–Oxygen Battery Fiber with High Energy Density. *Angew. Chem. Int. Ed.* **2017**, *56*, 13741–13746. [[CrossRef](#)] [[PubMed](#)]
23. Jian, Z.; Yang, N.; Vogel, M.; Leith, S.; Schulte, A.; Schönherr, H.; Jiao, T.; Zhang, W.; Müller, J.; Butz, B.; et al. Flexible Diamond Fibers for High-Energy-Density Zinc-Ion Supercapacitors. *Adv. Energy Mater.* **2020**, *10*, 2002202. [[CrossRef](#)]
24. Luo, Y.; Zhang, Y.; Zhao, Y.; Fang, X.; Ren, J.; Weng, W.; Jiang, Y.; Sun, H.; Wang, B.; Cheng, X.; et al. Aligned carbon nanotube/molybdenum disulfide hybrids for effective fibrous supercapacitors and lithium ion batteries. *J. Mater. Chem. A* **2015**, *3*, 17553–17557. [[CrossRef](#)]
25. Li, H.; Liu, Z.; Liang, G.; Huang, Y.; Zhu, M.; Pei, Z.; Xue, Q.; Tang, Z.; Wang, Y.; Li, B.; et al. Waterproof and Tailorable Elastic Rechargeable Yarn Zinc Ion Batteries by a Cross-Linked Polyacrylamide Electrolyte. *ACS Nano* **2018**, *12*, 3140–3148. [[CrossRef](#)]
26. Zhang, Q.; Li, C.; Li, Q.; Pan, Z.; Sun, J.; Zhou, Z.; He, B.; Man, P.; Xie, L.; Kang, L.; et al. Flexible and High-Voltage Coaxial-Fiber Aqueous Rechargeable Zinc–Ion Battery. *Nano Lett.* **2020**, *19*, 4035–4042. [[CrossRef](#)] [[PubMed](#)]
27. Pan, Z.; Yang, J.; Li, L.; Gao, X.; Kang, L.; Zhang, Y.; Zhang, Q.; Kou, Z.; Zhang, T.; Wei, L.; et al. All-in-one stretchable coaxial-fiber strain sensor integrated with high-performing supercapacitor. *Energy Storage Mater.* **2019**, *25*, 124–130. [[CrossRef](#)]
28. Zhang, Y.; Wang, Y.; Wang, L.; Lo, C.-M.; Zhao, Y.; Jiao, Y.; Zheng, G.; Peng, H. A fiber-shaped aqueous lithium ion battery with high power density. *J. Mater. Chem. A* **2016**, *4*, 9002–9008. [[CrossRef](#)]
29. Shukla, A.; Venugopalan, S.; Hariprakash, B. Nickel-based rechargeable batteries. *J. Power Sources* **2001**, *100*, 125–148. [[CrossRef](#)]
30. Lu, Y.; Chen, J. Prospects of organic electrode materials for practical lithium batteries. *Nat. Rev. Chem.* **2020**, *4*, 127–142. [[CrossRef](#)]
31. Cui, J.; Guo, Z.; Yi, J.; Liu, X.; Wu, K.; Liang, P.; Li, Q.; Liu, Y.; Wang, Y.; Xia, Y.; et al. Organic Cathode Materials for Rechargeable Zinc Batteries: Mechanisms, Challenges, and Perspectives. *ChemSuschem* **2020**, *13*, 2160–2185. [[CrossRef](#)]
32. Wang, H.; Liu, Z.; Ding, J.; Lepró, X.; Fang, S.; Jiang, N.; Yuan, N.; Wang, R.; Yin, Q.; Lv, W.; et al. Downsized sheath-core conducting fibers for weavable superelastic wires, biosensors, supercapacitors, and strain sensors. *Adv. Mater.* **2016**, *28*, 4998–5007. [[CrossRef](#)]
33. Lima, M.D.; Fang, S.; Lepró, X.; Lewis, C.; Ovalle-Robles, R.; Carretero-González, J.; Castillo-Martínez, E.; Kozlov, M.E.; Oh, J.; Rawat, N.; et al. Biscrolling Nanotube Sheets and Functional Guests into Yarns. *Science* **2011**, *331*, 51–55. [[CrossRef](#)] [[PubMed](#)]

34. Chakkaravarthy, C.; Periasamy, P.; Jegannathan, S.; Vasu, K. The nickel/iron battery. *J. Power Sources* **1991**, *35*, 21–35. [[CrossRef](#)]
35. Shukla, A.; Ravikumar, M.; Balasubramanian, T. Nickel/iron batteries. *J. Power Sources* **1994**, *51*, 29–36. [[CrossRef](#)]
36. Zhang, M.; Fang, S.; Zakhidov, A.A.; Lee, S.B.; Aliev, A.E.; Williams, C.D.; Atkinson, K.R.; Baughman, R.H. Strong, transparent, multifunctional, carbon nanotube sheets. *Science* **2005**, *309*, 1215–1219. [[CrossRef](#)]
37. Guan, C.; Wang, Y.; Hu, Y.; Liu, J.; Ho, K.H.; Zhao, W.; Fan, Z.; Shen, Z.; Zhang, H.; Wang, J. Conformally deposited NiO on a hierarchical carbon support for high-power and durable asymmetric supercapacitors. *J. Mater. Chem. A* **2015**, *3*, 23283–23288. [[CrossRef](#)]
38. Ke, Q.; Zheng, M.; Liu, H.; Guan, C.; Mao, L.; Wang, J. 3D TiO₂@Ni(OH)₂ Core-shell Arrays with Tunable Nanostructure for Hybrid Supercapacitor Application. *Sci. Rep.* **2015**, *5*, 1–11. [[CrossRef](#)] [[PubMed](#)]
39. Lin, T.W.; Dai, C.S.; Hung, K.C. High energy density asymmetric supercapacitor based on NiOOH/Ni₃S₂/3D graphene and Fe₃O₄/graphene composite electrodes. *Sci. Rep.* **2014**, *4*, 1–10. [[CrossRef](#)] [[PubMed](#)]
40. Liu, Z.; Tay, S.W.; Li, X. Rechargeable battery using a novel iron oxide nanorods anode and a nickel hydroxide cathode in an aqueous electrolyte. *Chem. Commun.* **2011**, *47*, 12473–12475. [[CrossRef](#)]
41. Kim, S.-K.; Kim, H.J.; Lee, J.-C.; Braun, P.V.; Park, H.S. Extremely Durable, Flexible Supercapacitors with Greatly Improved Performance at High Temperatures. *ACS Nano* **2015**, *9*, 8569–8577. [[CrossRef](#)] [[PubMed](#)]
42. Chao, D.; Xia, X.; Liu, J.; Fan, Z.; Ng, C.F.; Lin, J.; Zhang, H.; Shen, Z.X.; Fan, H.J. A V₂O₅/conductive-polymer core/shell nanobelt array on three-dimensional graphite foam: A high-rate, ultrastable, and freestanding cathode for lithium-ion batteries. *Adv. Mater.* **2014**, *26*, 5794–5800. [[CrossRef](#)] [[PubMed](#)]
43. Wang, H.; Liang, Y.; Gong, M.; Li, Y.; Chang, W.; Mefford, T.; Zhou, J.; Wang, J.; Regier, T.; Wei, F.; et al. An ultrafast nickel-iron battery from strongly coupled inorganic nanoparticle/nanocarbon hybrid materials. *Nat. Commun.* **2012**, *3*, 1–8. [[CrossRef](#)] [[PubMed](#)]
44. Huo, G.; Lu, X.; Huang, Y.; Li, W.; Liang, G. Electrochemical Performance of α -Fe₂O₃ Particles as Anode Material for Aqueous Rechargeable Batteries. *J. Electrochem. Soc.* **2014**, *161*, A1144–A1148. [[CrossRef](#)]
45. Jin, Z.; Li, P.; Jin, Y.; Xiao, D. Superficial-defect engineered nickel/iron oxide nanocrystals enable high-efficient flexible fiber battery. *Energy Storage Mater.* **2018**, *13*, 160–167. [[CrossRef](#)]
46. Li, X.; Gao, T.; Liu, Q.; Xu, Y.; Li, J.; Xiao, D. Designing a high-performance anode composed of carbon nanotubes and Fe-Fe₃C nanoparticles for quasi-solid-state fibrous Ni/Fe batteries. *Mater. Chem. Front.* **2021**, *5*, 3636–3645. [[CrossRef](#)]
47. Li, Q.; Zhang, Q.; Liu, C.; Sun, J.; Guo, J.; Zhang, J.; Zhou, Z.; He, B.; Pan, Z.; Yao, Y. Flexible all-solid-state fiber-shaped Ni-Fe batteries with high electrochemical performance. *J. Mater. Chem. A* **2019**, *7*, 520–530. [[CrossRef](#)]
48. Guan, C.; Zhao, W.; Hu, Y.; Ke, Q.; Li, X.; Zhang, H.; Wang, J. High-Performance Flexible Solid-State Ni/Fe Battery Consisting of Metal Oxides Coated Carbon Cloth/Carbon Nanofiber Electrodes. *Adv. Energy Mater.* **2016**, *6*, 1601034. [[CrossRef](#)]
49. Zhu, J.; Zhang, Q.; Yang, S.; Chen, L.; Zhao, P.; Yan, Q. Anode Electrodeposition of Fe/Fe₃O₄ composite on Carbon Fabric as a Negative Electrode for Flexible Ni-Fe Batteries. *ChemElectroChem* **2021**, *8*, 4817–4825. [[CrossRef](#)]
50. Li, P.; Jin, Z.; Xiao, D. A phytic acid etched Ni/Fe nanostructure based flexible network as a high-performance wearable hybrid energy storage device. *J. Mater. Chem. A* **2017**, *5*, 3274–3283. [[CrossRef](#)]
51. Li, X.; Guo, Y.; Gao, T.; Li, P.; Jin, Z.; Xiao, D. Interconnecting 3D Conductive Networks with Nanostructured Iron/Iron Oxide Enables a High-Performance Flexible Battery. *ACS Appl. Mater. Interfaces* **2021**, *13*, 57411–57421. [[CrossRef](#)] [[PubMed](#)]
52. Yang, J.; Zhang, Q.; Wang, Z.; Wang, Z.; Kang, L.; Qi, M.; Chen, M.; Liu, W.; Gong, W.; Lu, W.; et al. Rational Construction of Self-Standing Sulfur-Doped Fe₂O₃ Anodes with Promoted Energy Storage Capability for Wearable Aqueous Rechargeable NiCo-Fe Batteries. *Adv. Energy Mater.* **2020**, *10*, 2001064. [[CrossRef](#)]
53. Kong, D.; Wang, Y.; Huang, S.; Zhang, B.; Von Lim, Y.; Sim, G.J.; Valdivia Alvarado, P.; Ge, Q.; Yang, H.Y. 3D Printed Compressible Quasi-Solid-State Nickel-Iron Battery. *ACS Nano* **2020**, *14*, 9675–9686. [[CrossRef](#)] [[PubMed](#)]

Disclaimer/Publisher's Note: The statements, opinions and data contained in all publications are solely those of the individual author(s) and contributor(s) and not of MDPI and/or the editor(s). MDPI and/or the editor(s) disclaim responsibility for any injury to people or property resulting from any ideas, methods, instructions or products referred to in the content.